Published manuscript at https://doi.org/10.1016/j.medengphy.2022.103836

Self-expandable stent for thrombus removal modeling: solid or beam finite elements?

Giulia Luraghi[1], Sara Bridio[1], Francesco Migliavacca[1] and Jose Felix Rodriguez Matas[1]

[1]Department of Chemistry, Materials and Chemical Engineering, Politecnico di Milano, Piazza L. da Vinci 32, 20133 Milan, Italy

Corresponding author

Giulia Luraghi, PhD

Computational Biomechanics Laboratory – LaBS

Department of Chemistry, Materials and Chemical Engineering 'Giulio Natta'

Politecnico di Milano

Piazza L. da Vinci 32, 20133 Milan, Italy

Tel: +39.02.2399.3399

Email address: giulia.luraghi@polimi.it

Abstract

Background - The performance of self-expandable stents is being increasingly studied by means of finite-element analysis. As for peripheral stents, transcatheter valves and stent-grafts, there are numerous computational studies for setting up a proper model, this information is missing for stent-retrievers used in the procedure of thrombus removal in cerebral arteries. It is well known that the selection of the appropriate finite-element dimensions (topology) and formulations (typology) is a fundamental step to set up accurate and reliable computational simulations. In this context, a thorough verification analysis is here proposed, aimed at investigating how the different element typologies and topologies - available to model a stent-retriever - affect simulation results.

Method - Hexahedral and beam element formulations were analyzed first individually by virtually replicating a crimping test on the device, and then by replicating the thrombectomy procedure aiming at removing a thrombus from a cerebral vessel. In particular, three discretization refinements for each element type and different element formulations including both full and reduced integration were investigated and compared in terms of the resultant radial force of the stent and the stress field generated in the thrombus.

Results - The sensitivity analysis on the element formulation performed with the crimping simulations allowed the identification of the optimal setting for each element family. Both setting lead to similar results in terms of stent performance in the virtual thrombectomy and should be used in future studies simulating the mechanical thrombectomy with stent-retrievers.

Conclusions - The carried out virtual thrombectomy procedures confirmed that the beam element formulation results were sufficiently accurate to model the radial force and the performance of the stent-retriever during the procedure. For different self-expandable stents, hexahedral formulation could be essential in stress analysis.

Keywords: FEA, FEM, verification, in silico, thrombectomy

1 Introduction

The constantly improving and increasing popularity of the endovascular treatments for acute ischemic stroke (AIS) allowed a new stent family to appear in the clinical application. In particular, stent-retrievers were developed [1] aimed at improving the success rate of recanalization in AIS patients, and their efficacy was demonstrated in different clinical trials [2–6]. Stent-retrievers are self-expandable devices made of nickel-titanium alloys, a superelastic material which, once crimped with high deformations, can return to its original shape by simply removing the constraints during the mechanical thrombectomy procedure. The crimped stent is positioned with minimally invasive access in the AIS location, where a thrombus blocks the brain perfusion. Once the stent is correctly positioned with respect to the thrombus location by means of a guide catheter, it is deployed by removing the catheter sheath and it mechanically entraps the thrombus in its cells; even at this stage, the expanded stent may restore the blood flow by compressing the thrombus between the stent-retriever and the arterial wall. Finally, the stent and the thrombus complex are retrieved along the vessel towards a receiving catheter.

In the design, optimization, and performance analysis of an endovascular stent, the use of finite element analysis is widely used. A detailed numerical analysis could be required by regulatory agencies to approve a new biomedical device [7]. Moreover, the recent publication of the ASME V&V 40-2018 focuses on how to assess the credibility of a medical device computational model through the verification and validation process [8]. The verification process aims at verifying that the numerical model accurately solves the required mathematical model [9]. Two different concepts are involved: i) verification of the implemented equations in the numerical solver and ii) minimization of the numerical error. While the former step can be assumed as already verified if commercial software is used (as in this study), the latter is a crucial aspect to be considered and discussed each time a numerical stent model is proposed.

The numerical error is the difference between the numerical and the unknown true solution of the equations, unavoidable because of the spatial discretization of the domain where the equations need to be solved [9].

In the specific case of stent retrievers, literature is quite scarce on numerical models because of the relative novelty of the devices and of the mechanical thrombectomy procedure itself [10]. Gu et al modeled a non-commercial stent-retriever to evaluate the strain and stress fields and the resultant radial force during its deployment in a cylindrical vessel and its contact with a thrombus [11,12]. Liu et al. developed a finite element model to simulate the stent-retriever thrombectomy procedure and to investigate the device-clot contact [13]. In our previous works, we modeled commercial stent-retrievers during virtual thrombectomy procedures to validate the model by reproducing in vitro experiments [14] and a real patient-specific case [15,16]. A verification study on the stent-retrievers is not available in the literature, and also verification studies on stents, in general, are few [17–19].

This work is aimed at investigating how the choice of the finite elements formulation affects the modeling results of the behavior of stent retrievers. The three-dimensional continuum element and the one-dimensional beam element families are exhaustively analyzed and compared by reproducing a radial compression test. As a final case of comparison, one formulation for each finite element family is selected and used to perform a virtual thromboectomy simulation (a real application of the stent retriever). The main hypothesis that we want to prove in this work is that the beam element formulation is sufficiently accurate to capture the radial force and to model the performance of the stent-retriever during the procedure.

2 Methods

2.1 Finite-elements overview

The finite element method allows to obtain a solution for not analytically solvable partial differential equations, turning them into a more accessible system of algebraic equations. The method consists in numerically solving a mathematical model, describing a given physical system, based on equations and boundary conditions. The equations are solved within the elements in which the continuum spatial domain is discretized. There are different families of elements (named *topology*), grouped according to their dimensionality: one-dimensional elements (truss and beam), two-dimensional elements (membrane and shell), and three-dimensional elements (tetrahedral, prism, hexahedral, and pentahedral). Truss and membrane elements differ from beam and shell elements because they cannot support loads in shear and bending. Furthermore, in each element family, different formulations (named *typology*) are available, and the number and location of the integration points can vary. The dimension of the adopted elements is usually chosen according to the geometry of the domain, while the formulation and number of integration points are set according to the specific applied loading conditions. Primary variables (displacements, velocities, and accelerations) are solved and stored on nodes, while stresses and strains require integration on the element volume which is usually performed by means of Gaussian quadrature. In the literature, the majority of the stent and stent-retriever models consider beam elements [14,20–22] or hexahedral elements [11–13,23–28].

2.2 Stent-retriever model

In this study, the Trevo ProVue (Stryker Corporation, Michigan, USA) with a nominal diameter of 4 mm, working length of 20 mm, total length of 40 mm and cross-section of 69x69 μm^2 was modeled (figure 1a). It is a self-expanding, laser-cut, nitinol stent-retriever, whose geometry is characterized by an open-cell design and a spiral nature of cell pattern [29].

A high-fidelity three-dimensional model of the stent was created by means of SolidWorks 2020 (Dassault Systemes SolidWorks Corp., Waltham, MA, USA). The planar sketch was obtained by replicating the elementary cell unit cell. The final 3D CAD model was obtained by wrapping the planar sketch and was exported together with its centerline. Both the 3D and the centerline geometries were discretized with ANSA Pre Processor v21.0 (BETA CAE System, Switzerland) in hexahedral (figure 1b) and beam (figure 1c) elements respectively (further discretization details are in the following section).

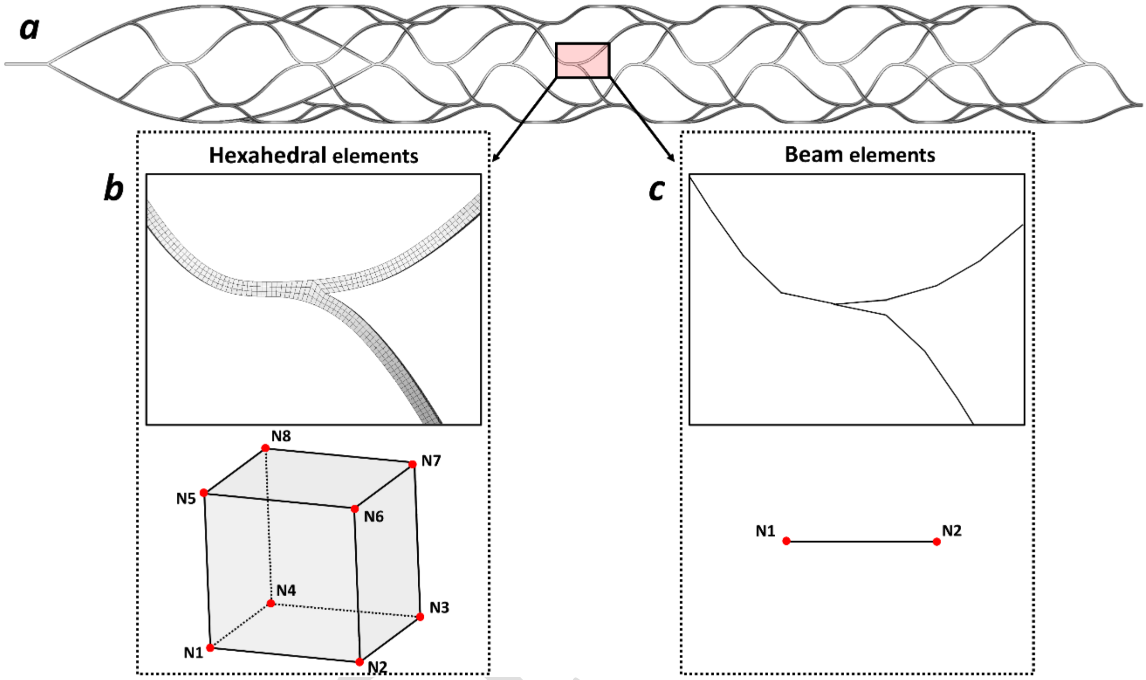

Figure 1: stent-retriever geometry (a) discretized with both hexahedral 8-node elements (b) and beam 2-node elements (c).

The nitinol shape memory alloy was modeled with a superelastic material law. Material calibration was previously performed through a numerical-experimental coupling as described in our previous work [14]. The complete list of material parameters is in Table 1.

Table 1: nitinol material parameters

Parameter	Meaning	Value
ρ	Mass density	6.45 g/cm^3
EA	Austenite elastic modulus	45 GPa
EM	Martensite elastic modulus	17 GPa

ν	Poisson's ratio	0.3
σ_{AM}^{S}	Starting stress forward phase transformation	365 MPa
σ_{AM}^{F}	Final stress forward phase transformation	386 MPa
σ_{MA}^{S}	Starting stress reverse phase transformation	197 MPa
σ_{MA}^{F}	Final stress reverse phase transformation	156 MPa
ε	Recoverable strain	0.048

2.3 Element size and formulation sensitivity analysis

Different element sizes were considered for both the analyzed finite-element families. For each family, three different element resolutions were compared. In particular, for the hexahedral grids, the squared section of the stent-retriever was discretized in 2x2, 3x3, and 4x4 elements and the complete grids of the device were obtained by fixing the hexahedral element size (models **H**2, **H**3, **H**4). As regards the beam grids, the centerline of the device was discretized with beam elements with an average length of 0.6 mm, 0.3 mm, and 0.15 mm (models **B**06, **B**03, **B**015). The mean element size and the total element counting of each model are reported in Table 2.

Different hexahedral element typologies were examined in the element formulation sensitivity analysis. First, in models **LF** a linear (first-order) fully integrated formulation was considered. It counts 8 integration points where stress and strain are calculated. It is not suffering from volumetric locking, but the typical shear locking could increase the stiffness of these elements in the bending-dominated problem [30]. In the advanced linear fully integrated formulation (models **LF$^{\mathbf{Adv}}$**) a modified strain approach resolves the shear locking behavior in bending problems (another similar advanced linear fully integrated formulation is also known as incompatible mode formulations) [31]. In model **QF,** the quadratic (second-order) fully integrated formulation was used because of its better performance in bending-dominated problems, at the expense of a higher computational cost. Models **LR** present linear reduced integrated formulations with only one integration point and the consequent hourglassing modes (also called zero-energy modes) to be controlled. Three hourglasses controls were here investigated: the viscous damping [32] (models **LR^{hgV}**), the elastic stiffness [33] (models **LR^{hgS}**), and finally the Puso control [34] (models **LR^{hgP}**).

As regards the 2-node beam element typology, only the Hughes-Liu formulation [35] was compatible with the adopted shape memory alloy material model (in the used commercial finite element solver). For the sake of completeness, an alternative formulation (with other material models) would be the Belytschko-Schwer cross-section integration [36]. The integration for the beam element is performed with one point of integration along the axis and multiple points in the cross-section. For the rectangular cross-sections, 2x2, 3x3, and 4x4 Gauss quadrature formulations were here investigated and compared (models **2G, 3G, 4G**). The beam has no zero-energy or locking modes. The complete overview of the investigated hexahedral and beam formulations is presented in Table 2.

Table 2: Hexahedral and beam models for the sensitivity study

Element size sensitivity analysis			
Model	Element typology	Element size (mm)	Total number of elements
H2	Hexahedral	0.0345	28,240
H3	Hexahedral	0.023	96,246
H4	Hexahedral	0.0175	228,528
B06	Beam	0.6	455
B03	Beam	0.3	865
B015	Beam	0.15	1,730
Element formulation sensitivity analysis			
Model	Element typology	Formulation	
H…-LF	Hexahedral	Linear fully integrated	
H…-LF^{Adv}	Hexahedral	Advanced linear fully integrated	
H…-QF	Hexahedral	Quadratic fully integrated	
H…-LR^{hgV}	Hexahedral	Linear reduced integrated with viscous hourglass	
H…-LR^{hgS}	Hexahedral	Linear reduced integrated with stiffness hourglass	
H…-LR^{hgP}	Hexahedral	Linear reduced integrated with Puso hourglass	

B…-2G	Beam	Hughes-Liu with 2x2 Guass points in the section
B…-3G	Beam	Hughes-Liu with 3x3 Guass points in the section
B…-4G	Beam	Hughes-Liu with 4x4 Guass points in the section

2.4 Crimping test and thrombectomy deployment simulations settings

The crimping test aims at measuring the radial compression force of the device. It was designed to resemble the effect of a radial compression machine [37]. In this regard, twelve rigid planes were used to mimic the machine and a radial displacement of 1.25 mm on each plane was prescribed to reduce the stent diameter from 4.0 mm (figure 2a-c) to 1.5 mm (figure 2b-d). Penalty self-contact between the struts of the stent was considered to prevent inter-penetration. The interaction between the rigid planes (master parts) and the external face of the device (slave part) was modeled as a rough penalty contact with a friction value of 0.1. A mass proportional damping of 1 s^{-1} was adopted for the stent in order to achieve stability without excessively constraining the maximum time step [38]. A selective mass-scaling was used in order to have a constant time-step of 1e-6 s. The von Mises (VM) stresses were also averaged in two different stent sections and used as compared variable between solid and beam elements models.

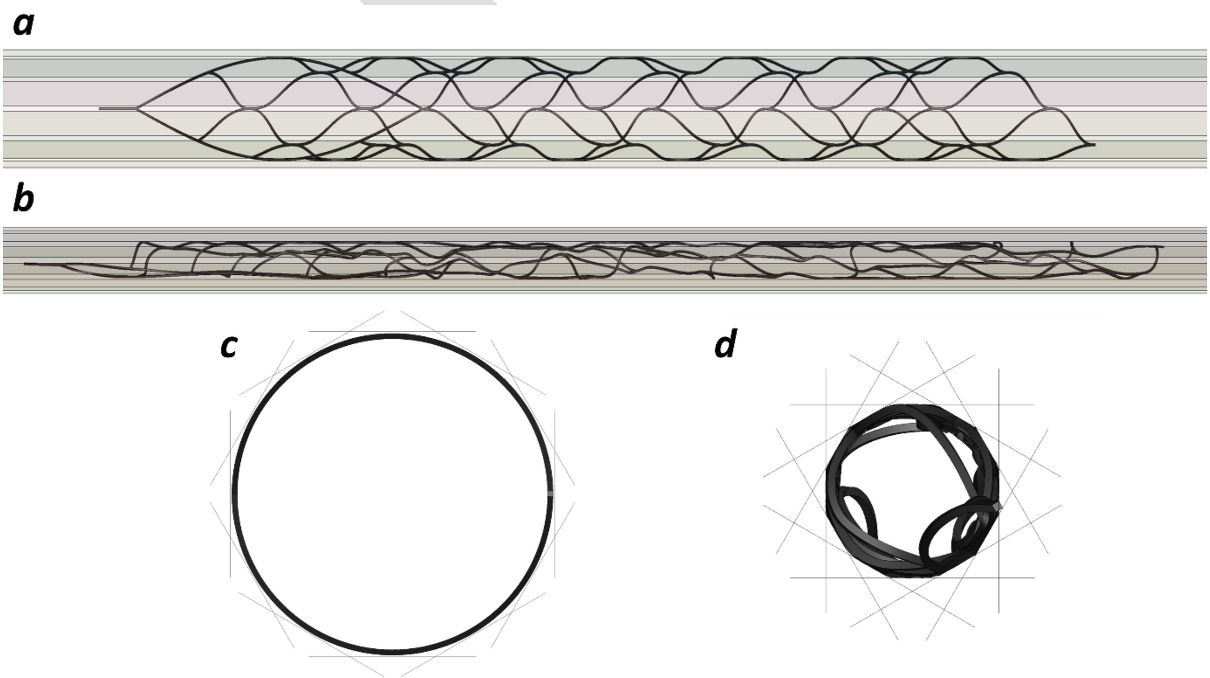

Figure 2: Crimping simulation in which the stent-retriever diameter is reduced from 4 mm (a-c) to 1.5 mm (b-d) by twelve rigid planes moving in the radial direction

The thrombectomy deployment simulation aims at reproducing the initial deployment of the stent retriever where the contact with the clot looks like in the real clinical application. A detailed description of the in-silico procedure can be found in [14]. An idealized straight vessel and an average clot (in terms of composition and length) were chosen for the purpose of this study. The straight vessel was modeled as a rigid cylinder with a diameter of 2.80 mm [39] and a length of 80 mm. The diameter was chosen according to the middle cerebral artery mean diameter, as the most common location for acute ischemic stroke [40]. The clot has a length of 14 mm [41], a composition 35% erythrocytes - 65% fibrin composition [42], and 95% occlusive diameter. It was discretized with tetrahedral elements and modeled as a compressible foam material. The catheter (to position the crimped stent) was modeled as a 0.5 mm diameter rigid straight cylinder. The vessel, catheter, and clot were discretized with ANSA Pre Processor v21.0 (BETA CAE System, Switzerland). The clot material was modeled with a quasi-hyperelastic foam formulation by fitting stress-strain curves from in vitro tests on ex vivo clots as described elsewhere [14,15]. Mass proportional damping of 1 s^{-1} was adopted for both the stent and the clot. A selective mass-scaling was adopted in order to have a constant time-step of 5e-7 s. The von Mises (VM) stresses on the clot during the deployment phase were analyzed in order to compare the two topology stent models.

All finite element simulations were performed on 20 CPUs of an Intel Xeon64 with 120 GB of RAM using the commercial explicit finite element solver LS-DYNA 971 Release 12.0 (ANSYS, Canonsburg, PA, USA). The quasi-static condition in all the simulations was achieved with a ratio between the kinetic and the internal energy of less than 1%.

3 Results

3.1 Crimping test – Solid formulations

The crimping test was numerically performed on the stent models and the resultant radial compression forces were measured and used as a comparison variable between the investigated 8-node hexahedral element formulations (figure 3). Two metrics have been used: i) a direct comparison of the Force-Diameter curve for each stent, and ii) the value of the radial force at specific crimping diameters.

In general, the differences between different formulations are more visible in the coarse mesh H2. As the mesh becomes finer, the results between different formulations became closer, as shown in figure 3, where curves from H4 do overlap. Regarding the H2 models, LF and LF^{Adv} present no important difference in terms of the resultant force. Both the linear fully integrated formulations result stiffer with respect to the quadratic formulation QF, of about 4.7% (calculated as the difference between the resultant radial force curves). The LR-models results differ based on the hourglass formulation. In particular, the LR^{hgV} model failed to converge, while both the elastic stiffness LR^{hgS} and Puso LR^{hgP} formulations worked correctly. The LR^{hgS} model, similarly to LF and LF^{Adv} models, results stiffer than the LR^{hgP}, which provides results similar to the QF model. LR^{hgS} and LR^{hgP} force curves differ by at most 4.4%. Another important difference between LR models is the hourglass dissipation energy, which is 35% higher in LR^{hgS} with respect to LR^{hgP}. The same comparison trends between different element formulations are observed in H3 and H4 models, but with progressively smaller percentage differences. As an example, the maximum difference between models LF^{Adv} and LR^{hgP} in terms of the resultant force is 4.3%, 3.7%, and 2.1% for H2, H3, and H4 respectively. Regarding the computational time, differences were not observed between the two LF models and between the two LR models. QF model (for all the grid refinements) results, as expected, the most expensive (about + 73% with respect to LF models), while the LR models were the fastest (about – 41% with respect to LF models) for all the considered grid refinements.

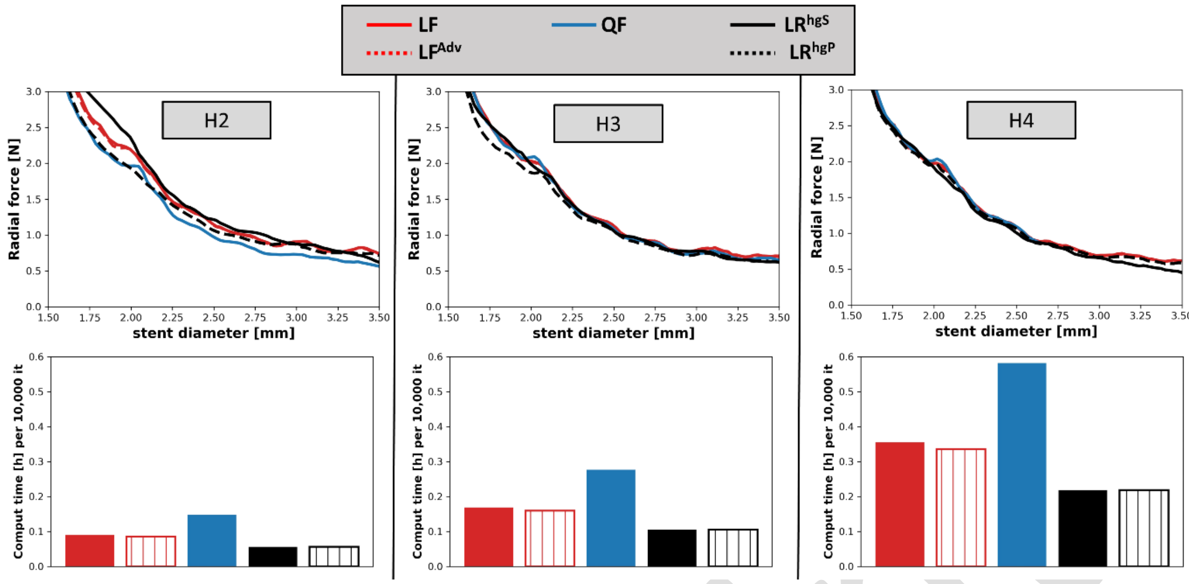

Figure 3: comparison between different element formulations for each considered refinement grid (H2, H3, and H4) in terms of radial force vs stent diameter curves and computational time to solve 10,000 iterations.

A mesh size sensitivity analysis was conducted on the LR^{hgP} models by comparing radial force and averaged VM stress curves. The three girds (H2, H3, and H4 models) show similar results in terms of radial forces (figure 4a), with a percentage difference of less than 3.7% between H2 and H4 and 1.4% between H3 and H4. The VM stresses were averaged in two different stent regions as shown in figure 4. Region 1 is located in the middle of a straight strut (figure 4c), whereas region 2 is located at the junction of two struts (figure 4d). The differences in terms of averaged VM between grid refinements are below 7% for crimp diameters between 1.5 mm and 2.75mm, with an increase up to 48% for crimp diameters in the 2.75 mm-3.5 mm range. In region 2, H2 and H3 give the same VM stress (differences below 3%) while the H4 stress curve shows lower values with a difference of up to 28% with respect to H2 and H3. Radial force and VM stress values at 1.75 mm, 2.5 mm, and 3.75 mm of stent diameter are reported in table 3. The computational time increased, as expected, with the mesh refinement with a +87% from H2 to H3 and + 107% from H3 to H4 (figure 4b).

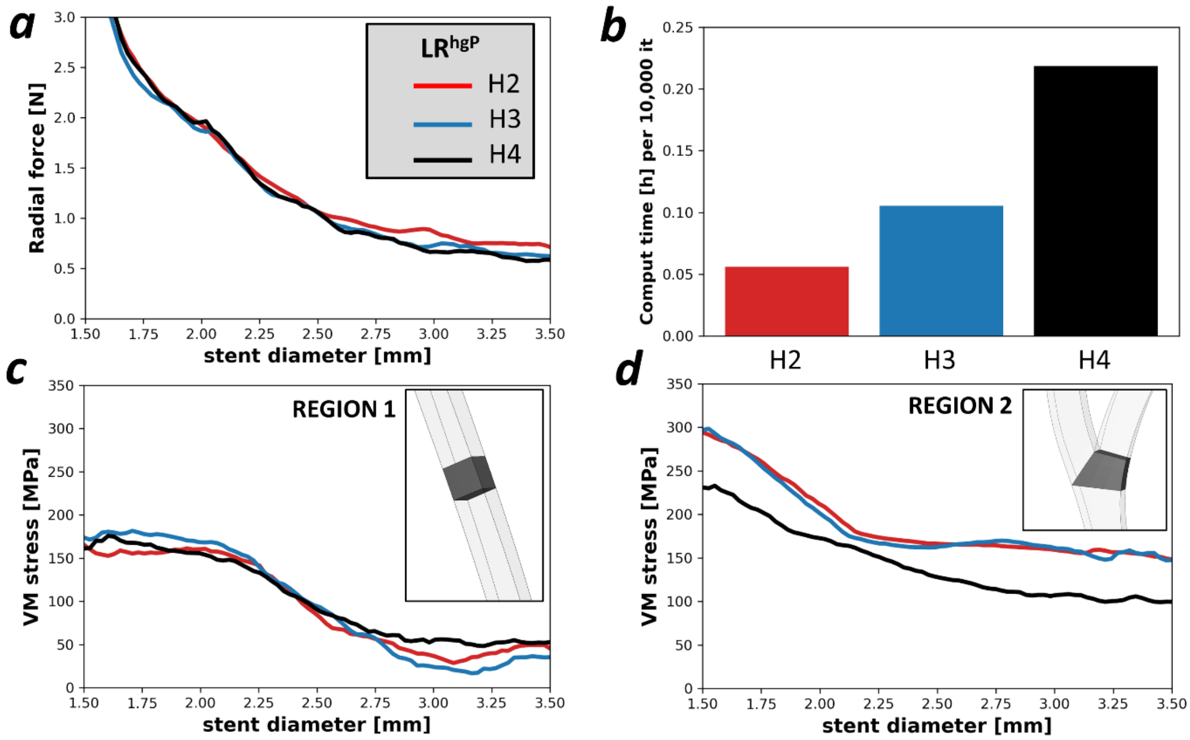

Figure 4: mesh size sensitivity analysis on the hexahedral models. H2- LR^{hgP}, H3- LR^{hgP} and H4- LR^{hgP} were compared in terms of radial force curves (a), computational time to solve 10,000 iterations (b) and averaged VM stresses (c-d). Region 1 is located in the middle of a straight strut, while region 2 is where two struts join.

3.2 Crimping test – Beam formulations

A different number of Gauss points, 2G, 3G, and 4G are used to integrate the stress field in the section of beam elements, and three different element sizes 0.6 mm (B06), 0.3 mm (B03), and 0.15 mm (B015) are investigated (see Table 2). In model B06, the difference between the radial force curves for the 2G and 4G models is less than 1% whereas the 3G model gives a 7.5% lower radial force with respect to the other two models (figure 5). In models B03 and B015, the difference between 2G and 4G models is less than 1.5%, whereas the radial force curves for the 3G model are 4.6% and 4.3% lower for B03 and B015 respectively. The computational time increased, as expected, with the increasing number of Gaussian points in the cross-section, with a +12% from 2G to 3G and + 11% from 3G to 4G.

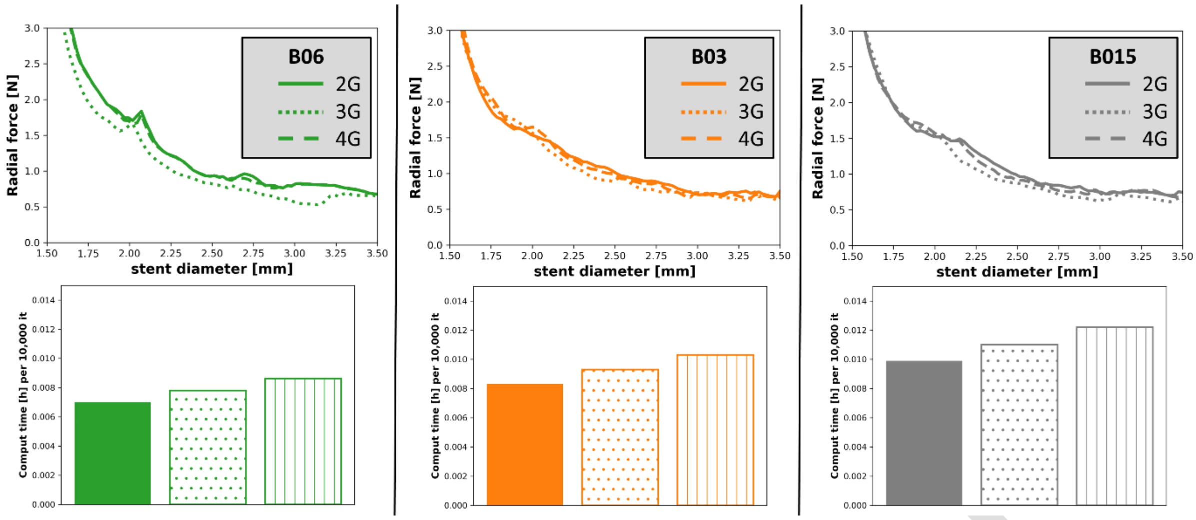

Figure 5: comparison between different element formulations for each considered refinement grid (B06, B03, and B015) in terms of radial force vs stent diameter curves and computational time to solve 10,000 iterations.

The -2G models were chosen to run the beam size sensitivity analysis where the resulting radial force and averaged VM stress curves were compared. Regarding the radial force (figure 6a) models B03 and B015 show similar results with a percentage difference of less than 5%. On the contrary, model B06 was stiffer (in particular for crimp diameters lower than 2 mm) with a resulting radial force higher than 11%. As for the solid models, two different regions were selected for the averaged VM stress evaluation, the first in the middle of a straight strut (figure 6c), and the second at the junction of two struts (figure 6d). Differences were found in both regions, more important in region 2. In region 1, the averaged stress curves result in differences up to 16% for crimp diameters between 1.5mm and 2.1 mm. For crimp diameters between 2.1 mm and 3.5 mm, the differences were reduced to only 5%. The differences between grid refinements in region 2 are greater especially between models B06 and the others (B03 and B015), with a maximum percentage difference of 22%. Radial force and VM stress values at 1.75 mm, 2.5 mm, and 3.75 mm of stent diameter are reported in table 3. The computational time increased, as expected, with the mesh refinement, with a +19% both from B06 to B03 and from B03 to B015 (figure 6b).

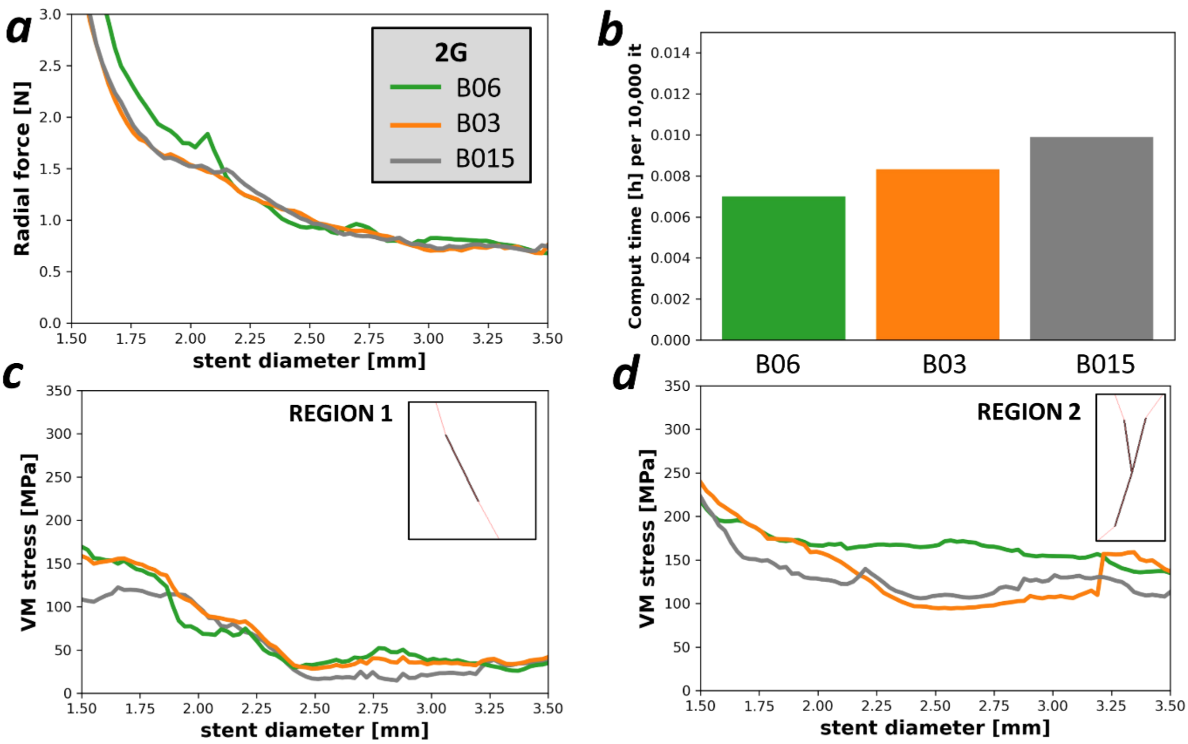

Figure 6: mesh size sensitivity analysis on the beam models. B06-2G, B03-2G and B015-2G were compared in terms of radial force curves (a), computational time to solve 10,000 iterations (b) and averaged VM stresses (c-d). Region 1 is located in the middle of a straight strut, while region 2 is where two struts join.

3.3 Crimping test – Solid and Beam elements comparison

A comparison in terms of radial force and VM stress in regions 1 and 2 at different stent diameters between the three LR^{hgP} solid models and the three 2G beam models is reported in table 3. In general the beam formulation lead a lower average radial force and VM stress than the solid formulation indicating a lower stiffness for the beam elements. However, the differences in the radial force between the solid and beam element formulation is found to be less than 12% at the lower crimping diameter, with a difference of less than 5% for diameters between 2.5mm and 3.75mm. Table 3 also shows that the stress distribution in regions 1 and 2 is not uniform, as indicated by the standard deviation of the VM stress. However, it is noticed that the standard deviation to average ratio is the same for all solid cases (0.3) and beam cases (0.6). This indicates that even the coarser meshes are able to capture the heterogeneity of the stress and strain field within the regions. The intermediate refinement grid of the solid topology H3-LR^{hgP} results in a radial force higher than 11%, 5%, and 6% at 1.75 mm, 2.50 mm, and 3.75 mm stent diameters respectively, with respect to the intermediate refinement grid of the beam topology B03-2G. As for the averaged VM stresses, the percentage differences increase to 20%, 66%, and 45% at the three stent diameters in region 1 and to 27%, 41%, and 27% in region 2. However, it should be noted that the comparison of volume-averaged stress between solid and beam models is not consistent, because regions 1 and 2 present different volumes in solid and beam models due to the different grid resolutions. Regarding the computing time, the beam based models result in mo re efficient scheme with a total wall time ratio for models B03-2G and H3-LR^{hgP} of 1:11.

Table 3: comparison in terms of radial force (RF), VM stress in region 1 (VMS^1) and in region 2 (VMS^2) at different stent diameters (1.75 mm, 2.50 mm, and 3.75 mm) between hexahedral (H2-LR^{hgP}, H3-LR^{hgP,} H4-LR$^{hgP)}$ and beam (B06-2G, B03-2G, B015-2G) models.

Model	d=1.75 mm			d=2.50 mm			d=3.75 mm		
	RF [N]	**VMS^1 [MPa]**	**VMS^2 [MPa]**	**RF [N]**	**VMS^1 [MPa]**	**VMS^2 [MPa]**	**RF [N]**	**VMS^1 [MPa]**	**VMS^2 [MPa]**
H2-LR^{hgP}	2.37	155±114	259±73	1.10	87±26	166±48	0.59	29±22	95±24
H3-LR^{hgP}	2.28	178±131	253±77	1.08	95±30	162±48	0.50	21±15	98±24
H4-LR^{hgP}	2.41	165±126	201±60	1.08	92±25	129±37	0.47	41±10	78±18
B06-2G	2.29	149±28	182±107	0.93	28±4	116±63	0.44	30±8	81±32
B03-2G	2.03	142±25	183±106	1.02	32±5	95±51	0.47	38±11	71±29

B015-2G	2.05	119±24	149±88	1.01	17±2	108±60	0.50	14±4	78±31

3.4 Stent-retriever deployment simulation

Models H3-LR^{hgP} and B03-2G were used in the thrombectomy initial deployment simulation and a comparison in terms of VM stress in the clot is here proposed. Both the stent-retriever models worked properly (with no error) in the simulations composed of crimping, positioning, and deployment steps as visible in figure 7a. The VM stress in the clot has been considered a variable directly related to the stent radial force performance. The mark of the stent-retriever on the clot is visible and is similar for both models (figure 7b). The maximum VM stress curves for both models are reported in figure 7c. The average of the 10 elements with the maximum value, instead of local maximum values, is considered in order to avoid possible spikes due to the contact of the clot with the stent or due to excessive distortion of the mesh. The maximum percentage difference between models H3-LR^{hgP} and B03-2G is 6%, corresponding to the final phase of the deployment step.

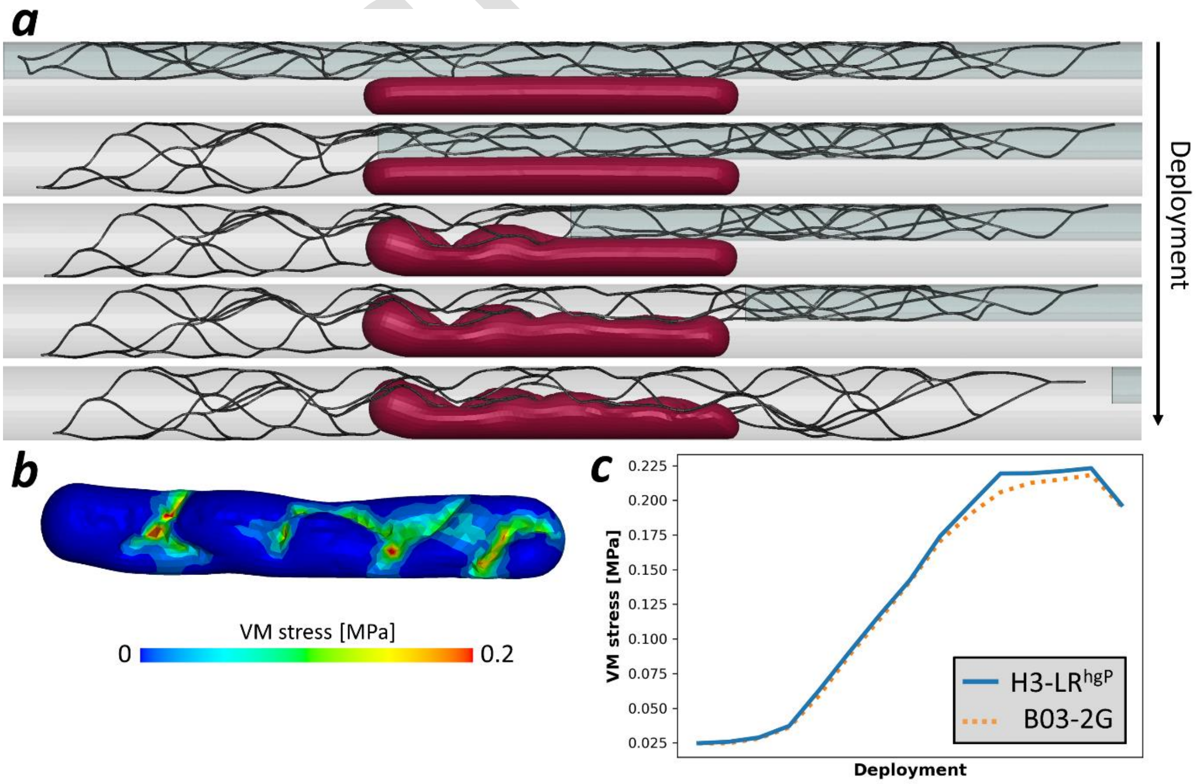

Figure 7: simulation of stent-retriever deployment (a), mark of the stent-retriever on the clot at the end of the deployment and von Mises stress contour plot (b), comparison of the maximum von Mises stress (average of the 10 most stresses elements) during the deployment step with the chosen hexahedral and beam formulations (c).

Discussion

In recent years, finite element analysis has been considered a useful tool in both engineering and clinical applications to design and optimize new devices, but also to reproduce virtual implantation in virtual patients. Several finite-element studies on stents, peripheral or carotid stents, on transcatheter aortic valves or endovascular stent-grafts can be found in the literature [11,12,27,28,14,20–26]. However, only a few [17–19] concerning a rigorous verification analysis on stent modeling. This work focuses on a new family of self-expandable stents, namely stent-retrievers, used in the endovascular mechanical removal of blood clots in case of AIS. Stent-retrievers are still rarely studied since they are being developed at a rapid pace. To date, stent retrievers have been models using two different finite elements: i) incompatible hexahedral solid elements [11–13], and ii) Hughes-Liu beam elements [14,15]. However, none of these studies have conducted a sensitivity analysis on elements typology and topology.

A thorough verification analysis is here proposed, aimed at investigating how the different element typologies and topologies -available to model a stent-retriever- affect the simulation results. Hexahedral and beam element formulations were analyzed first individually by virtually replicating a crimping test on the device, and then they were compared both in the same test and in an idealized thrombectomy test (final application of the device).

Starting from the solid elements models, different formulations and element sizes were compared in terms of resulting radial force and averaged VM stress. Between the linear reduced integrated formulations, the optimum choice is the model with the Puso hourglass control because it entails the lowest hourglass dissipation energy with the same computational time. Between the linear fully integrated formulations, the advanced (or incompatible) formulation must be preferred because it resolves the shear locking behavior in bending problems with the same computational time as the classical linear fully integrated formulation. The use of a quadratic fully integrated formulation is not here justified, because of an important increment in computational time only small differences in terms of results are obtained. As expected, differences between formulations decrease for increasingly fine grids. The comparison in terms of averaged VM stresses is quite difficult to perform because results can change considerably by looking at different locations in the stent locations and by considering different volumes in which the average is calculated. When dealing with local stress analysis in stent models to evaluate the fatigue behavior, different sections at different locations should be considered if the stress analysis is the focus of the numerical analysis. Different models give non-negligible differences which must be considered during element size and typology sensitivity analysis if the resulting stress values are important for the purpose of the simulation. As regards the beam elements models, percentage differences always less than 5% were detected by varying the number of Gauss points in the cross-section of the beam element. For this reason, the fastest 2x2 Gauss points model was chosen as the preferable formulation within the Hughes-Liu beam family. The same non-convergent VM stress curve behavior observed in the solid models is also here detected.

The sensitivity analysis on the element formulation performed with the crimping simulations allowed the indication of two preferred formulations within different element typology (one for each family, hexahedral and beam). They are the H3-LR^{hgP} and B03-2G models. The last part of this study aimed at comparing these two selected formulations during an in silico idealized thrombectomy. Stress fields on the clot were used to evaluate the performance of the

Published manuscript at https://doi.org/10.1016/j.medengphy.2022.103836

stent-retriever models during the virtual deployment. Important differences were not detected between models H3-LR^{hgP} and B03-2G.

The comparison between the selected solid and beam elements highlights how the different typologies (solid vs beam) can affect the simulation results replicating crimping and thrombectomy tests. As indicated by previous studies in the literature [17,18], the beam elements formulation turns out effective (with differences with the solid formulation less than 5%) for applications where only kinematics and radial force are important as for the thrombectomy procedure (with differences with the solid formulation less than 6%), or if rapid results are needed at the expense of accuracy. The carried out virtual thrombectomy procedures confirmed that the beam element formulation is enough to model the stent-retriever performance during the procedure.

Differently, if the stress and strain fields are important for engineering and manufacturing applications, solid elements are suggested [19] or at least a more detailed sensitivity analysis is strongly recommended. These considerations obtained with a specific stent-retriever can be generalized and applied to different stent designs and applications.

This study is aimed at proposing a proof-of-concept methodology to carry out sensitivity analysis on stent models, in particular on stent-retrievers to choose the most appropriate element (typology and topology) for the type of analysis to be performed. The present study shows that the typology and topology sensitivity analyses turned out to be enough to capture the kinematic and the overall device performance (i.e. radial force) but were unsatisfactory for a detailed analysis of the stress and strain fields. However, a thorough validation analysis with experiments, missing in this study, will be required to fully assess the accuracy and appropriateness of the element choice. Further, if the scope of the numerical analysis is the study of local stresses and strains in case of fatigue behavior prediction, a more involved sensitivity, and statistical analysis than that herewith proposed is needed. Lastly, the specific formulations investigated in this study for each topology are limited to the choice of the adopted commercial software; different commercial or in-house software might present different implemented formulations.

In conclusion, the importance of assessing the reliability and truthfulness of numerical models is well known and a strict verification analysis is always needed [43]. This is particularly true for stent modeling where the stent design and applications can change significantly, affecting the element typology and topology choice. In general, mesh refinements should be high enough to accurately represent the actual geometry of the device, while the appropriate typology and topology selection depends on the objective of the particular analysis under consideration.

Sources of funding

This study has received funding from the European Union's Horizon 2020 research and innovation program under grant agreement No 777072 and from the MIUR FISR-FISR2019_03221 CECOMES.

Declaration of competing interest

The authors declare that they have no known competing financial interests or personal relationships that could have appeared to influence the work reported in this paper.

Acknowledgments

The authors thank Lorenzo Agnoli and Andrea Cassinerio for their precious contribution in the simulations running.

Bibliography

[1] Kühn AL, Vardar Z, Kraitem A, King RM, Anagnostakou V, Puri AS, et al. Biomechanics and hemodynamics of stent-retrievers. J Cereb Blood Flow Metab 2020;40:2350–65. https://doi.org/10.1177/0271678X20916002.

[2] Berkhemer OA, Fransen PSS, Beumer D, Van den Berg LA, Lingsma HF, Yoo AJ, et

al. A Randomized Trial of Intraarterial Treatment for Acute Ischemic Stroke. N Engl J Med 2015;372:11–20. https://doi.org/10.1056/NEJMoa1411587.

[3] Goyal M, Demchuk AM, Menon BK, Eesa M, Rempel JL, Thornton J, et al. Randomized Assessment of Rapid Endovascular Treatment of Ischemic Stroke. N Engl J Med 2015;372:1019–30. https://doi.org/10.1056/nejmoa1414905.

[4] Saver JL, Goyal M, Bonafe A, Diener H-C, Levy EI, Pereira VM, et al. Stent-Retriever Thrombectomy after Intravenous t-PA vs. t-PA Alone in Stroke. N Engl J Med 2015;372:2285–95. https://doi.org/10.1056/NEJMoa1415061.

[5] Campbell BCV, Mitchell PJ, Kleinig TJ, Dewey HM, Churilov L, Yassi N, et al. Endovascular Therapy for Ischemic Stroke with Perfusion-Imaging Selection. N Engl J Med 2015;372:1009–18. https://doi.org/10.1056/NEJMoa1414792.

[6] Jovin TG, Chamorro A, Cobo E, de Miquel MA, Molina CA, Rovira A, et al. Thrombectomy within 8 Hours after Symptom Onset in Ischemic Stroke. N Engl J Med 2015;372:2296–306. https://doi.org/10.1056/NEJMoa1503780.

[7] Viceconti M, Pappalardo F, Rodriguez B, Horner M, Bischoff J, Musuamba Tshinanu F. In silico trials: Verification, validation and uncertainty quantification of predictive models used in the regulatory evaluation of biomedical products. Methods 2020;185:120–7. https://doi.org/10.1016/j.ymeth.2020.01.011.

[8] The American Society of Mechanical Engineers. Assessing Credibility of Computational Modeling Through Verificationa and Validation: Application to Medical Devices 2018. See https://www.asme.org/codes-standards/find-codes-standards/v-v-40-assessing-credibility-computational-modeling-verification-validation-application-medical-devices

[9] Pathmanathan P, Gray RA. Ensuring reliability of safety-critical clinical applications of computational cardiac models. Front Physiol 2013;4:358.

https://doi.org/10.3389/fphys.2013.00358.

[10] Luraghi G, Cahalane RME, van de Ven E, Overschie SCM, Gijsen FJH, Akyildiz AC. In vitro and in silico modeling of endovascular stroke treatments for acute ischemic stroke. J Biomech 2021;127:110693. https://doi.org/10.1016/j.jbiomech.2021.110693.

[11] Gu X, Qi Y, Erdman AG. The Wall Apposition Evaluation for a Mechanical Embolus Retrieval Device. J Heal Eng 2018:2018:9592513. https://doi.org/10.1155/2018/9592513.

[12] Gu X, Qi Y, Erdman A, Li Z. The role of simulation in the design of a semi-enclosed tubular embolus retrieval. J Med Devices, Trans ASME 2017;11:0210011–7. https://doi.org/10.1115/1.4036286.

[13] Liu R, Jin C, Wang L, Yang Y, Fan Y, Wang W. Simulation of stent retriever thrombectomy in acute ischemic stroke by finite element analysis. Comput Methods Biomech Biomed Engin 2021. https://doi.org/10.1080/10255842.2021.1976761.

[14] Luraghi G, Rodriguez Matas JF, Dubini G, Berti F, Bridio S, Duffy S, et al. Applicability assessment of a stent-retriever thrombectomy finite-element model. Interface Focus 2021;11:20190123. https://doi.org/10.1098/rsfs.2019.0123.

[15] Luraghi G, Bridio S, Rodriguez Matas JF, Dubini G, Boodt N, Gijsen FJH, et al. The first virtual patient-specific thrombectomy procedure. J Biomech 2021;126:110622. https://doi.org/10.1016/J.JBIOMECH.2021.110622.

[16] Bridio S, Luraghi G, Rodriguez Matas JF, Dubini G, Giassi GG, Maggio G, et al. Impact of the Internal Carotid Artery Morphology on in silico Stent-Retriever Thrombectomy Outcome. Front Med Technol 2021;0:40. https://doi.org/10.3389/FMEDT.2021.719909.

[17] Capelli C, Biglino G, Petrini L, Migliavacca F, Cosentino D, Bonhoeffer P, et al. Finite element strategies to satisfy clinical and engineering requirements in the field of

percutaneous valves. Ann Biomed Eng 2012;40:2663–73. https://doi.org/10.1007/s10439-012-0617-1.

[18] Hall GJ, Kasper EP. Comparison of element technologies for modeling stent expansion. J Biomech Eng 2006;128:751–6. https://doi.org/10.1115/1.2264382.

[19] Frischkorn J, Reese S. Solid-beam finite element analysis of nitinol stents. Comput Methods Appl Mech Eng 2015;291:42–63. https://doi.org/10.1016/J.CMA.2015.03.011.

[20] Zaccaria A, Migliavacca F, Pennati G, Petrini L. Modeling of braided stents: Comparison of geometry reconstruction and contact strategies. J Biomech 2020;107. https://doi.org/10.1016/j.jbiomech.2020.109841.

[21] Bosi GM, Capelli C, Cheang MH, Delahunty N, Mullen M, Taylor AM, et al. A validated computational framework to predict outcomes in TAVI. Sci Rep 2020;10:9906. https://doi.org/10.1038/s41598-020-66899-6.

[22] McGee OM, Gunning PS, McNamara A, McNamara LM. The impact of implantation depth of the Lotus™ valve on mechanical stress in close proximity to the bundle of His. Biomech Model Mechanobiol 2019;18:79–88. https://doi.org/10.1007/s10237-018-1069-9.

[23] Luraghi G, Matas JFR, Beretta M, Chiozzi N, Iannetti L, Migliavacca F. The impact of calcification patterns in transcatheter aortic valve performance: a fluid-structure interaction analysis. Comput Methods Biomech Biomed Engin 2020;14:1–9. https://doi.org/10.1080/10255842.2020.1817409.

[24] Mao W, Wang Q, Kodali S, Sun W. Numerical Parametric Study of Paravalvular Leak Following a Transcatheter Aortic Valve Deployment Into a Patient-Specific Aortic Root. J Biomech Eng 2018;140:1010071–10100711. https://doi.org/10.1115/1.4040457.

[25] Ghosh RP, Marom G, Bianchi M, D'souza K, Zietak W, Bluestein D. Numerical evaluation of transcatheter aortic valve performance during heart beating and its post-deployment fluid–structure interaction analysis. Biomech Model Mechanobiol 2020;19:1725–40. https://doi.org/10.1007/s10237-020-01304-9.

[26] Mazzaccaro D, Berti F, Antonini L, Pennati G, Petrini L, Migliavacca F, et al. Biomechanical interpretation of observed fatigue fractures of peripheral Nitinol stents in the superficial femoral arteries through in silico modelling. Med Hypotheses 2020;142:109771. https://doi.org/10.1016/j.mehy.2020.109771.

[27] Pasta S, Cannata S, Gentile G, Di Giuseppe M, Cosentino F, Pasta F, et al. Simulation study of transcatheter heart valve implantation in patients with stenotic bicuspid aortic valve. Med Biol Eng Comput 2020;58:815–29. https://doi.org/10.1007/s11517-020-02138-4.

[28] Wu W, Pott D, Mazza B, Sironi T, Dordoni E, Chiastra C, et al. Fluid–Structure Interaction Model of a Percutaneous Aortic Valve: Comparison with an In Vitro Test and Feasibility Study in a Patient-Specific Case. Ann Biomed Eng 2016;44:590–603. https://doi.org/10.1007/s10439-015-1429-x.

[29] Prince HC, Saliba AJ, Wheeler J, Bruder S. Development of the Trevo ProVue retriever for intracranial clot removal in acute ischemic stroke. Ann N Y Acad Sci 2014;1329:107–15. https://doi.org/10.1111/nyas.12579.

[30] Nagtegaal JC, Parks DM, Rice JR. On numerically accurate finite element solutions in the fully plastic range. Comput Methods Appl Mech Eng 1974;4:153–77. https://doi.org/10.1016/0045-7825(74)90032-2.

[31] Simo JC, Armero F. Geometrically non-linear enhanced strain mixed methods and the method of incompatible modes. Int J Numer Methods Eng 1992;33:1413–49. https://doi.org/10.1002/NME.1620330705.

[32] Kosloff D, Frazier GA. Treatment of hourglass patterns in low order finite element codes. Int J Numer Anal Methods Geomech 1978;2:57–72. https://doi.org/10.1002/nag.1610020105.

[33] Flanagan DP, Belytschko T. A uniform strain hexahedron and quadrilateral with orthogonal hourglass control. Int J Numer Methods Eng 1981;17:679–706. https://doi.org/10.1002/nme.1620170504.

[34] Puso MA. A highly efficient enhanced assumed strain physically stabilized hexahedral element. Int J Numer Methods Eng 2000;49:1029–64. https://doi.org/10.1002/1097-0207(20001120)49:8<1029::AID-NME990>3.0.CO;2-3.

[35] Hughes TJR, Liu WK. Nonlinear finite element analysis of shells-part II. two-dimensional shells. Comput Methods Appl Mech Eng 1981;27:167–81. https://doi.org/10.1016/0045-7825(81)90148-1.

[36] Belytschko T, Schwer L, Klein MJ. Large displacement, transient analysis of space frames. Int J Numer Methods Eng 1977;11:65–84. https://doi.org/10.1002/nme.1620110108.

[37] Katz JM, Hakoun AM, Dehdashti AR, Chebl AB, Janardhan V, Janardhan V. Understanding the Radial Force of Stroke Thrombectomy Devices to Minimize Vessel Wall Injury: Mechanical Bench Testing of the Radial Force Generated by a Novel Braided Thrombectomy Assist Device Compared to Laser-Cut Stent Retrievers in Simulated MCA Vessel Diameters. Interv Neurol 2019;8:206–14. https://doi.org/10.1159/000501080.

[38] Luraghi G, Migliavacca F, Rodriguez Matas JF. Study on the Accuracy of Structural and FSI Heart Valves Simulations. Cardiovasc Eng Technol 2018;9:1–16. https://doi.org/10.1007/s13239-018-00373-3.

[39] Davison MA, Ouyang B, Keppetipola KM, Chen M. Arterial diameter and the gender

disparity in stroke thrombectomy outcomes. J Neurointerv Surg 2018;10:949–52. https://doi.org/10.1136/neurintsurg-2017-013697.

[40] Dutra BG, Tolhuisen ML, Alves HCBR, Treurniet KM, Kappelhof M, Yoo AJ, et al. Thrombus Imaging Characteristics and Outcomes in Acute Ischemic Stroke Patients Undergoing Endovascular Treatment. Stroke 2019;50:2057–64. https://doi.org/10.1161/STROKEAHA.118.024247.

[41] Boodt N, Compagne KCJ, Dutra BG, Samuels N, Tolhuisen ML, Alves HCBR, et al. Stroke Etiology and Thrombus Computed Tomography Characteristics in Patients with Acute Ischemic Stroke: A MR CLEAN Registry Substudy. Stroke 2020;51:1727–35. https://doi.org/10.1161/STROKEAHA.119.027749.

[42] Staessens S, Fitzgerald S, Andersson T, Clarençon F, Denorme F, Gounis MJ, et al. Histological stroke clot analysis after thrombectomy: Technical aspects and recommendations. Int J Stroke 2020;15:467–76. https://doi.org/10.1177/1747493019884527.

[43] Roache PJ. Verification of Codes and Calculations. AIAA J 1998;36. https://doi.org/10.2514/2.457.